Mapping Floods in Urban Areas From Dual-Polarization InSAR Coherence Data

Ramona Pelich, *Member, IEEE*, Marco Chini, *Senior Member, IEEE*, Renaud Hostache, Patrick Matgen, Luca Pulvirenti, *Member, IEEE*, and Nazzareno Pierdicca, *Senior Member, IEEE*

***Abstract*— Previous studies have shown that the decrease of temporal interferometric synthetic aperture radar (InSAR) coherence could be exploited to detect the appearance of floodwater in urban areas. However, as of today, approaches based on this principle only make use of single co-polarization images for identifying the presence of floodwater in the double-bounce feature. In this study, we take advantage of both co- and cross-polarization images to detect significant decreases of the multitemporal InSAR coherence in order to enhance the mapping of floodwater in urban areas. We consider that not only double-bounce scattering, but also multiple-bounce may occur in urban areas depending on how the building facades are oriented with respect to the synthetic aperture radar (SAR) sensor's line of sight. The Sentinel-1 (S-1) mission is particularly well suited for applying and testing this kind of approach due to the systematic availability of dual-polarization data. Using as a test case, the widespread flooding in the city of Houston, USA, caused by Hurricane Harvey in 2017, we demonstrate that the proposed methodology leads to an increase of the accuracy of the urban flood maps from 75.2% when only using the VV polarization, to 82.9% when using the dual polarization information.**

***Index Terms*— Change detection, dual-polarization, flood maps, interferometric synthetic aperture radar (InSAR) coherence, synthetic aperture radar (SAR), urban areas.**

I. Introduction

NATURAL disasters due to hydrogeometeorological risks take place across the globe and affect different land classes, including urban areas, coastal zones, or agricultural lands. Urban flooding, in particular, represents a frequent and high-impact natural disaster, and one of its major causes are environmental changes such as sea level rise and more frequent extreme weather events [1]. To ensure an evidence-based and timely emergency response and damage assessment, flood extent maps are of paramount importance for disaster responders. Nowadays, the exploitation of an increasing availability of satellite earth observation (EO) data and the progress achieved in remote-sensing instruments enables a more accurate and efficient mapping of urban floods [2], [3]. SAR sensors occupy a privileged place among EO sensors due to their quasi-all-weather and day/night observation capabilities. Different studies propose algorithms enabling the detection of floods in urban areas from SAR observations [3]–[9].

In principle, due to the double-bounce scattering mechanism, the appearance of floodwater on roads in front of buildings becomes detectable when considering the increase of the SAR backscattering in the co-polarization channel [5]. However, when the building facades are not orthogonal to the satellite sensor's line of sight (LoS), the recorded increase of the SAR backscattering may not be sufficient for enabling the detection of floodwater. In order to overcome this limitation, Chini *et al.* and Pulvirenti *et al.* [4], [6] have proposed to take advantage of the interferometric synthetic aperture radar (InSAR) coherence feature in order to complement the SAR intensity. The underlying hypothesis of their proposed method is that the decrease of the co-event InSAR coherence with respect to the pre-event one reveals the appearance of floodwater in urban areas. Successful applications based on very high-resolution (VHR) COSMO-SkyMed images have shown the high potential of exploring observations of the InSAR coherence in addition to SAR intensity. InSAR coherence [10] and interferometric phase statistics [11] derived from VHR L-band SAR imagery acquired by the ALOS-2 satellite mission have also been used for urban floodwater monitoring. A fully automated algorithm capable of mapping urban floodwater by using C-band SAR data with decametric spatial resolution from the S-1 satellite mission has been introduced in [3]. The study exploits the short temporal and perpendicular baselines of the S-1 image pairs, thereby demonstrating their suitability for an effective InSAR coherence-based flood detection. Recently, research studies have proposed machine learning methods for the delineation of floodwater in urban areas. In [8], an unsupervised approach has been proposed by making use of SAR intensity and InSAR coherence under a Bayesian network fusion framework using S-1 data. In [12], an active self-learning convolution neural network (CNN) exploits SAR intensity and InSAR coherence extracted from TerraSAR-X data, while Rudner *et al.* [13] presented a CNN approach that performs a rapid segmentation of buildings by fusing multiresolution, multisensor, and multitemporal satellite imagery including S-1 InSAR coherence data.

All the above-mentioned SAR-based urban flood mapping approaches rely on single polarization images, namely the

Manuscript received May 22, 2021; revised July 30, 2021; accepted August 24, 2021. Date of publication September 15, 2021; date of current version December 23, 2021. This work was supported in part by the Luxembourg National Research Fund (FNR) through the Combining eArth obServation with a large-scale model Cascade for Assessing flood hazarD at high spatial rEsolution (CASCADE) Grant C17/SR/11682050 and the MOnitoring and predicting urban flood using Sar InTerferometric Observations (MOSQUITO) Grant C15/SR/10380137. *(Corresponding author: Ramona Pelich.)*

Ramona Pelich, Marco Chini, Renaud Hostache, and Patrick Matgen are with the Department of Environmental Research and Innovation (ERIN), Luxembourg Institute of Science and Technology (LIST), L-4422 Belvaux, Luxembourg (e-mail: ramona.pelich@list.lu; marco.chini@list.lu; renaud.hostache@list.lu; patrick.matgen@list.lu).

Luca Pulvirenti is with the CIMA Research Foundation, I-17100 Savona, Italy (e-mail: luca.pulvirenti@cimafoundation.org).

Nazzareno Pierdicca is with the Department of Information Engineering, Electronics and Telecommunications (DIET), Sapienza University of Rome, I-00184 Rome, Italy (e-mail: nazzareno.pierdicca@uniroma1.it).

Digital Object Identifier 10.1109/LGRS.2021.3110132

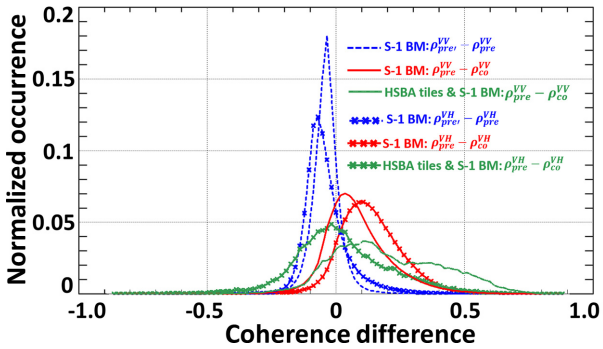

Fig. 1. Distributions of the InSAR coherence difference.

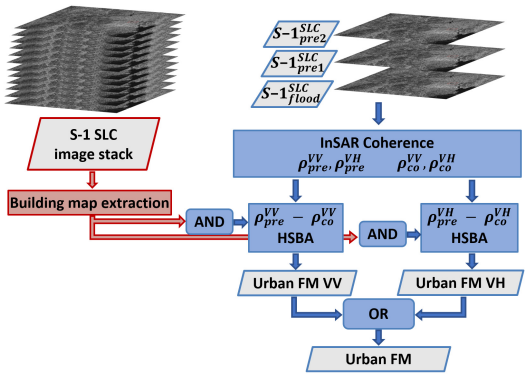

Fig. 2. Flowchart of the proposed algorithm.

co-polarization channel. Indeed, urban areas tend to be highly complex where, depending on the orientation of the buildings with respect to the SAR LoS, the backscattering intensity can be recorded differently in the co- and cross-polarization channels. To evaluate the contribution of both polarizations in detecting the presence of floodwater in urbanized areas, the S-1 mission is particularly well suited since it systematically acquires dual-polarization data in the VV-VH configurations.

II. Methodology

Generally, buildings have different orientation angles with respect to the SAR looking direction and, as a result, their corresponding backscattering signature is influenced by the polarimetric configuration of the radar [14]. For instance, the double-bounce scattering for an illumination orthogonal to the building alignment is caused by right-angled structures formed by building walls and roads, resulting in high and low backscattering values in the case of co-polarization and cross-polarization channels, respectively. Conversely, if the LoS and the building facades are not orthogonal, they create oblique angles, so that the contribution from cross-polarization becomes higher compared to the co-polarization one. For oblique incidence angles, the cross-polarized component is the result of multiple scattering from these man-made structures [15]. In this context, we assume that only using the co-polarization data could underestimate the extent of flooding in built up areas and, therefore, we propose to improve the floodwater detection by exploiting the multitemporal InSAR coherence from the cross-polarization channel. The novelty of this letter lies in using the InSAR coherence extracted from both the co- and cross-polarization channels for a more comprehensive delineation of floodwater in urban areas. The proposed methodology makes use of the findings from our previous study [3], demonstrating that the decrease of the InSAR multitemporal coherence indicates the appearance of floodwater in urban areas which are usually considered coherent targets. In order to detect the InSAR coherence drop-off, we propose a fully automatic and unsupervised classification approach. A prerequisite of the InSAR-based methodology is the SAR-based building map (BM). To this end, we make use of the approach proposed in [16] that employs S-1 multitemporal data for extracting the BM.

As previously mentioned, in order to detect buildings surrounded by floodwater, we use the InSAR coherence which measures the degree of correlation between two complex (phase and amplitude) images. S-1 is a well-suited mission for using InSAR coherence as an indicator of changes because the coherence degradation due to both spatial and temporal baselines is very low. Indeed, S-1 has a small and well-controlled orbital tube radius of 50 m, resulting in a small spatial baseline between image pairs. Moreover, the two S-1 satellites have a temporal baseline as short as six days. These two characteristics help containing the risk of an undesired coherence decrease over areas such as urban settlements which are supposed to be stable in time. In order to detect the coherence drop off caused by the appearance of floodwater in urban areas we propose to use: 1) an interferometric image pair composed of two images taken before the onset of the flood inundation from which we derive ρ_{pre} and 2) a pair constituted of one image taken before and another one acquired during the flood inundation from which we derive the coherence denoted ρ_{co}. In this framework, we make the following assumption: urban areas affected by a flood have $\rho_{\text{pre}} > \rho_{\text{co}}$. Fig. 1 illustrates the distribution of the coherence difference maps corresponding to the S-1 BM and computed for the flood case, that is, $\rho_{\text{pre}} - \rho_{\text{co}}$ (red curves). The distributions computed for the case of two image pairs acquired before the flood, $\rho_{\text{pre}'} - \rho_{\text{pre}}$ is also shown (blue curves). The latter are composed of values close to 0 since the temporal InSAR coherence over building areas is generally stable, while the flood coherence difference, $\rho_{\text{pre}} - \rho_{\text{co}}$, presents an important number of samples with values greater than 0 indicating that ρ_{co} is decreasing. The InSAR coherence difference characteristics can be noticed for both polarization channels despite the different absolute values of InSAR coherence, that is, the cross-pol coherence is lower than the co-pol coherence at the same acquisition geometry. Therefore, we hypothesize that the flood InSAR coherence difference map is composed of two classes, that is, one corresponding to the flood areas with values greater than 0 and one corresponding to nonflooded areas with values close to 0. Histogram thresholding or parametric approaches are commonly used to separate such distributions. However, the classification accuracy depends on the proportions of classes within the image and the overlap between the two classes, respectively. To overcome this limitation, we make use of a hierarchical split-based approach (HSBA) [17] that separates the classes of a bimodal distribution by identifying image tiles where the two distributions can be fit more reliably and accurately. The $\rho_{\text{pre}} - \rho_{\text{co}}$ distributions corresponding to the identified HSBA bimodal tiles, shown in Fig. 1 (green curves), depict the bimodal distributions that are classified by making use of a thresholding and region growing procedure.

The decrease of coherence is mapped from the double- and multiple-bounce features using VV and VH polarizations, respectively. Next, the two resulting maps are merged by using a logical OR function in the final map, denoted hereafter urban

TABLE I
CHARACTERISTICS OF THE INPUT DATASETS

	Input dataset	Date of acquisition	Resolution [m]	Characteristics
Building Map	S-1 IW images, orbit 143 VV-VH polarization	09/2016 and 08/2017	20	25 GRD images 6 SLC images
Flood Mapping InSAR Coherence	S-1 IW images, orbit 143 VV-VH polarization	pre-flood pair: 18 & 24/08/2017 co-event pair: 24 & 30/08/2017	20	3 SLC images, ρ sliding window: 5×5 pre-flood pair: B_t = 6 days, $B_\perp$ = 80.17 m co-event pair: B_t = 6 days, $B_\perp$ = 80.53 m
Validation data	GeoEye-1 VHR image	31 August 2017	0.46	12426 crowdsourcing points

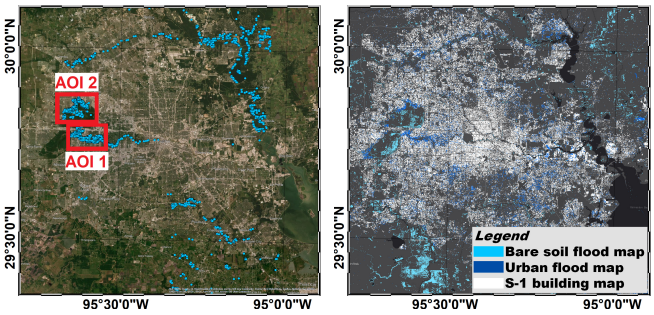

(a) (b)

Fig. 3. Experimental dataset overview, Houston (USA). (a) DG VHR imagery and crowdsourcing points. (b) S-1 UFM.

flood map (UFM). The entire procedure summarized in the flowchart given in Fig. 2 consists of the following main steps applied to both polarization channels:

1) BM detection (double and multiple bounces);
2) computation of $\rho_{\text{pre}} - \rho_{\text{co}}$;
3) HSBA detection of the InSAR coherence drop-off.

III. EXPERIMENTAL RESULTS

A. Datasets and Feature Extraction

The experimental results are based on an S-1 dataset acquired in the framework of Hurricane Harvey, which led to substantial large-scale flooding, affecting the metropolitan area of Houston, TX, in August and September 2017. In addition to the S-1 dataset, a GeoEye-1 VHR image was acquired on August 31, 2017, over Houston and was made available in the framework of the Digital Globe (DG) open data program. Thanks to the reduced cloud coverage at the acquisition time, DG's Tomnod crowdsourcing team was able to label the location of affected buildings over the city of Houston through photo interpretation, thereby providing a pointwise interpretation of these images, where each point depicts a building surrounded by floodwater. The resulting independent dataset is suitable for validating any SAR-based product. Fig. 3(a) gives an overview of the area of interest (AOI) addressed in the experimental results along with the DG crowdsourcing points.

The S-1 BM was derived from a multitemporal set of S-1 interferometric wide (IW) swath images spanning over one year from September 2016 to August 2017. The images were thus acquired before the landfall of hurricane Harvey. In order to detect a coherence drop off that can be related to the presence of floodwater, we made use of S-1 images acquired over the metropolitan area of Houston on August 30, 2017, when the flooding was still ongoing and close to its peak, as well as images acquired before the event. The SAR interferograms were generated from the SLC image pairs for each polarization channel separately. Table I summarizes the characteristics of the input data.

Fig. 3(b) gives the resulting UFM along with flooded bare soil areas mapped using the algorithm proposed in [17]. Fig. 4(d) showcases the contribution of both co- and cross-polarization channels in the UFM. One can notice that contributions of the two polarizations are indeed complementary and depend on the orientations of buildings with respect to SAR LoS depicted in Fig. 4(a), showing the red, green, and blue (RGB) composite of the multitemporal SAR intensities. An analogous behavior of the VV and VH roles is also demonstrated for the S-1 BM depicted in Fig. 4(b). Fig. 4(c) illustrates the RGB composite of VV and VH coherence drop offs corresponding to the flooded buildings. This result indicates that the contribution of each polarization channel is in accordance with the trend shown by the SAR intensity [Fig. 4(a)], that is, red areas are associated with a high decrease of VV InSAR coherence, blue areas with a high decrease of VH InSAR coherence, and white areas correspond to a high decrease for both polarizations. Moreover, one can notice that both VV and VH contributions to the final UFM from Fig. 4(d) show an agreement with the DG crowdsourcing points shown in Fig. 4(e), demonstrating the importance of using both polarization channels for a comprehensive SAR-based urban flood detection.

B. Discussion

First, we perform an in-depth qualitative analysis of the results corresponding to the two AOIs depicted in Fig. 3(a). In Fig. 5, we showcase the first AOI, a densely urbanized area as it can be observed from Fig. 5(d) and (e). From Fig. 5(a), showing the VV polarization SAR intensity as an RGB composite, one can notice that the presence of floodwater in urban areas leads to an increase of the backscattering in the flood image. However, the double-bounce increase is not sufficiently high to enable the identification of water in the SAR intensity domain. Therefore, the flooded buildings have been delineated by making use of the temporal change of InSAR coherence. Fig. 5(b) and (c) illustrates the multitemporal behavior of InSAR coherence over the same area for the VV and VH polarization channels, with an RGB composite ($R = \rho_{\text{pre}}$, $B = G = \rho_{\text{co}}$) image. We notice a significant change in the ρ values for both the co- and cross-polarization channels. In the urban areas affected by the flood, ρ decreases significantly, resulting in the condition $\rho_{\text{pre}} > \rho_{\text{co}}$, as depicted by areas in red color. We can further notice that some of the areas where the coherence decreases are the same for VV and VH. Fig. 5(f) showcases the common VV–VH flooded buildings depicted in dark blue as well as the flooded buildings delineated only by VV and only by VH illustrated in green and pink, respectively. This indicates a synergistic use of the two polarization channels for mapping urban floods. The VV–VH merged UFM is illustrated in Fig. 5(e) where the flooded buildings are depicted in dark blue. One can

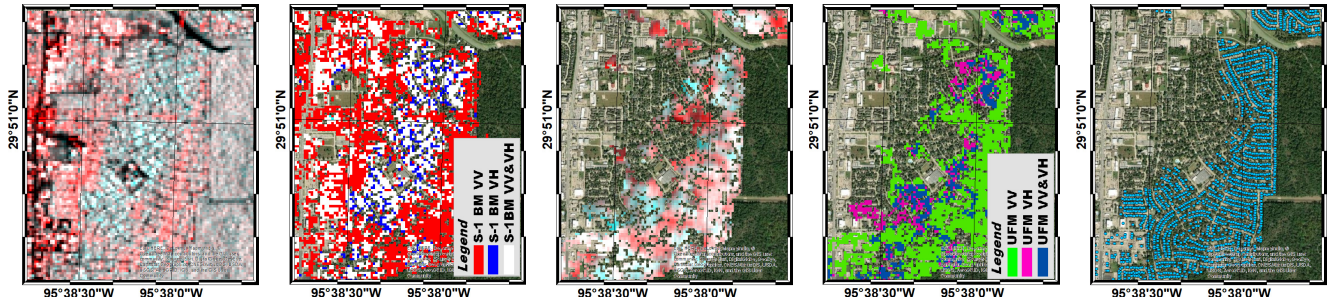

Fig. 4. VV and VH roles in (a) intensity temporal means ($R = \text{VV}$, $G = B = \text{VH}$, (b) S-1 BM). (c) Coherence drop-off ($R = \rho_{\text{pre}}^{\text{VV}} - \rho_{\text{co}}^{\text{VV}}$, $G = B = \rho_{\text{pre}}^{\text{VH}} - \rho_{\text{co}}^{\text{VH}}$). (d) VV-VH comparative UFM. (e) DG VHR imagery and flooded buildings crowd sourcing points.

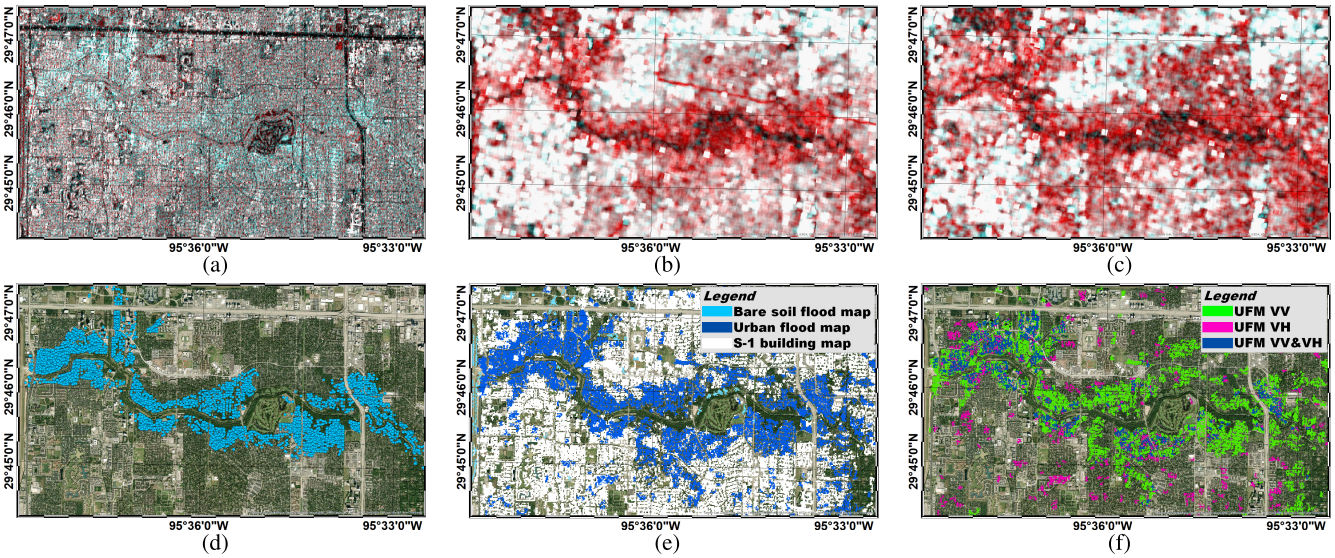

Fig. 5. AOI 1. (a) Intensity RGB composite: $R = 24/08/2017$, $B = G = 30/08/2017$. (b) VV and (c) VH InSAR ρ RGB composite: $R = \rho_{\text{pre}}^{18-24/08/2017}$, $B = G = \rho_{\text{co}}^{24-30/08/2017}$. (d) DG VHR imagery (31/08/2017) and crowd sourcing points of flooded buildings. (e) UFM (dark blue), flooded bare soil (light blue), nonflooded built-up areas (white). (f) VV–VH comparative UFM.

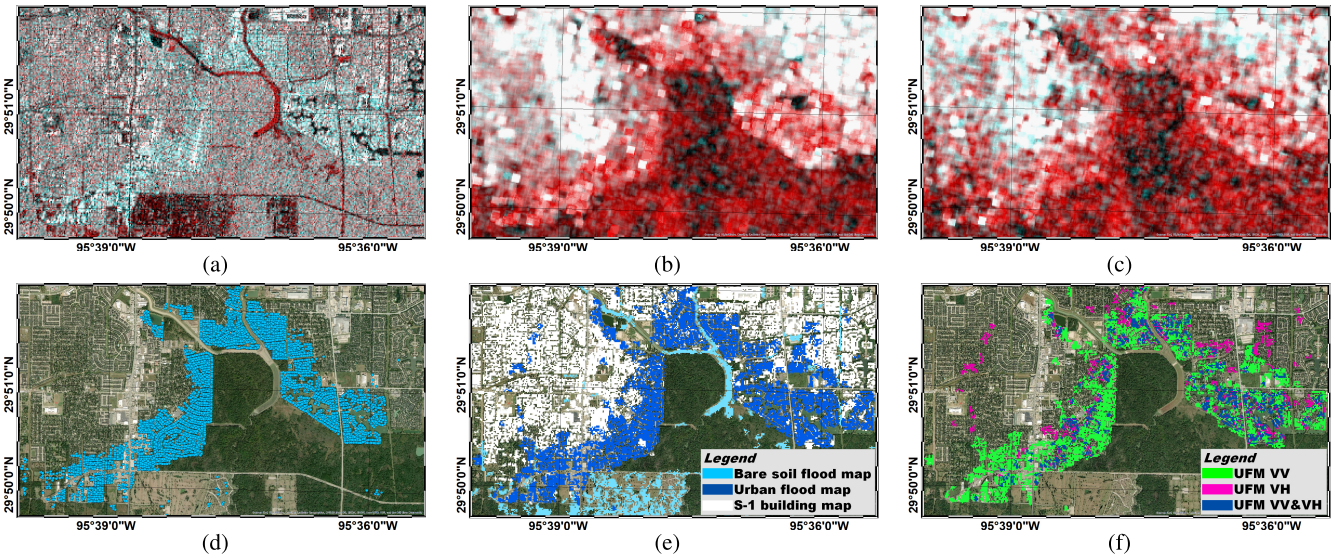

Fig. 6. AOI 2. (a) Intensity RGB composite: $R = 24/08/2017$, $B = G = 30/08/2017$. (b) VV and (c) VH InSAR ρ RGB composite: $R = \rho_{\text{pre}}^{18-24/08/2017}$, $B = G = \rho_{\text{co}}^{24-30/08/2017}$. (d) DG VHR imagery (31/08/2017) and crowd sourcing points of flooded buildings. (e) UFM (dark blue), flooded bare soil (light blue), nonflooded built-up areas (white). (f) VV–VH comparative UFM.

notice that the majority of the crowdsourced points shown in Fig. 5(d) depict the same areas as those identified by the coherence-based detection algorithm, as shown in Fig. 5(e). In addition, we observe from Fig. 5(f) that a significant part of the S-1-based UFM which is in agreement with the DG data are identified by VV only or by VH only. This confirms the necessity to combine the two polarizations in order to optimally exploit both double-bounce and multiple-bounce

TABLE II
S-1 AND DG QUANTITATIVE COMPARISON

S-1 UFM	***% wrt DG*** *(12426 points)*	***% wrt DG ∩ S-1 BM*** *(8120 points)*
VV (6109 points)	49.2 %	75.2%
VH (2743 points)	22.1 %	33.8%
VV OR VH (6728 points)	54.1 %	82.9%
VV AND VH (2124 points)	17.1 %	26.2%

scattering mechanisms in urban areas. By analyzing the second AOI illustrated in Fig. 6, we can notice that part of the urban floodwater is detected by the bare soil flood mapping algorithm and corresponds to areas where a significant backscattering drop-off is exhibited [Fig. 6(a)]. Analogous to the AOI 1 analysis, one can observe from Fig. 6(d) and (f) addressing AOI 2, that a low percentage of the S-1 flooded buildings validated by the DG dataset corresponds to the intersection of the VV and VH detections, thereby confirming the potential of a synergistic use of both polarization channels. In addition, we can also notice that not all the DG data points show corresponding detections in the S-1 UFM. A part of the apparent underdetection and overdetection can be explained by the difference in terms of spatial resolution between the S-1 data (20 m) and the DG image (0.46 m). We can also notice from Figs. 5(f) and 6(f) a slight overdetection of the S-1 flooded buildings resulting from both VV and VH channels with respect to the DG data points. The difference can be explained by the receding floodwater in the 24 h following the data acquisition or by surface changes that are not due to floodwater, for example, strong wind damages.

To quantitatively analyze the resulting UFMs, first, we have counted and resampled to the S-1 resolution the pixels that were labeled as flooded in the DG dataset, that is, 12 426 points. Then, we have counted how many of these pixels have been mapped as flooded by the proposed algorithm, for example, 6728 points for the merged VV-VH UFM. When analyzing the contributions of each polarization channel, one can notice that VV allows to detect a higher number of flooded buildings, namely 49%, with respect to VH that is only detecting 22% (Table II, second column). Their common detections correspond only to 17%, while their union reaches approximately 54%. This demonstrates the importance of using both co- and cross-polarizations to maximize the detection of floodwater presence in urbanized areas. The somewhat reduced number of points detected with the proposed approach could be explained by different acquisition times of the images, but also by the difference in spatial resolutions. For the proposed approach, the S-1 BM is a prerequisite and due to the lower S-1 spatial resolution, the intersection between DG points and the S-1 BM is composed of only 8120 points (65% of the total DG points). Considering only these buildings, the percentage of detection of flooded building reaches 82.9% for the merged VV-VH UFM (Table II, third column).

IV. CONCLUSION

An automatic algorithm enabling the mapping of floodwater in urban areas using 20-m resolution SAR data has been presented. It exploits the short temporal and spatial baselines of S-1 image pairs, as well as the intensity and the InSAR coherence from both VV and VH polarizations. Results show the added value of using cross-polarizations in addition to the more commonly used co-polarizations to detect floodwater in complex urban environments. Indeed, thanks to both polarizations, it is possible to fully exploit the InSAR coherence and its decrease in flood conditions where both double bounce and multiple bounce building returns are recorded. The algorithm was tested using the images acquired during the 2017 Atlantic hurricane season, which caused large-scale flooding in and around the city of Houston, USA. The obtained floodwater maps are quantitatively evaluated by a cross-comparison with DG crowdsourcing points, showing that the exploitation of both polarizations increases the capacity to detect floodwater around buildings by more than 5% compared to the exploitation of the co-polarization channel alone.

REFERENCES

[1] A. Jha *et al.*, "Five feet high and rising: Cities and flooding in the 21st century," World Bank Group, Washington, DC, USA, Policy Res. Work. Paper WPS 5648, 2011.
[2] S. I. Jiménez-Jiménez, W. Ojeda-Bustamante, R. E. Ontiveros-Capurata, and M. de Jesús Marcial-Pablo, "Rapid urban flood damage assessment using high resolution remote sensing data and an object-based approach," *Geomatics, Natural Hazards Risk*, vol. 11, pp. 906–927, May 2020.
[3] M. Chini, R. Pelich, L. Pulvirenti, N. Pierdicca, R. Hostache, and P. Matgen, "Sentinel-1 InSAR coherence to detect floodwater in urban areas: Houston and Hurricane Harvey as a test case," *Remote Sens.*, vol. 11, p. 107, Jan. 2019.
[4] M. Chini, L. Pulvirenti, and N. Pierdicca, "Analysis and interpretation of the COSMO-SkyMed observations of the 2011 Japan Tsunami," *IEEE Geosci. Remote Sens. Lett.*, vol. 9, no. 3, pp. 467–471, May 2012.
[5] D. C. Mason, L. Giustarini, J. García-Pintado, and H. L. Cloke, "Detection of flooded urban areas in high resolution synthetic aperture radar images using double scattering," *Int. J. Appl. Earth Observ. Geoinf.*, vol. 28, pp. 150–159, May 2014.
[6] L. Pulvirenti, M. Chini, N. Pierdicca, and G. Boni, "Use of SAR data for detecting floodwater in urban and agricultural areas: The role of the interferometric coherence," *IEEE Trans. Geosci. Remote Sens.*, vol. 54, no. 3, pp. 1532–1544, Mar. 2016.
[7] R. Natsuaki and A. Hirose, "L-band SAR interferometric analysis for flood detection in urban area—A case study in 2015 Joso flood, Japan," in *Proc. IEEE Int. Geosci. Remote Sens. Symp. (IGARSS)*, Jul. 2018, pp. 6592–6595.
[8] Y. Li, S. Martinis, M. Wieland, S. Schlaffer, and R. Natsuaki, "Urban flood mapping using SAR intensity and interferometric coherence via Bayesian network fusion," *Remote. Sens.*, vol. 11, p. 2231, Jan. 2019.
[9] L. Pulvirenti, M. Chini, and N. Pierdicca, "InSAR multitemporal data over persistent scatterers to detect floodwater in urban areas: A case study in Beletweyne, Somalia," *Remote. Sens.*, vol. 13, p. 37, Jan. 2021.
[10] R. Natsuaki and H. Nagai, "Synthetic aperture radar flood detection under multiple modes and multiple orbit conditions: A case study in Japan on Typhoon Hagibis, 2019," *Remote. Sens.*, vol. 12, p. 903, Jan. 2020.
[11] M. Ohki, T. Tadono, T. Itoh, K. Ishii, T. Yamanokuchi, and M. Shimada, "Flood detection in built-up areas using interferometric phase statistics of PALSAR-2 data," *IEEE Geosci. Remote Sens. Lett.*, vol. 17, no. 11, pp. 1904–1908, Nov. 2020.
[12] Y. Li, S. Martinis, and M. Wieland, "Urban flood mapping with an active self-learning convolutional neural network based on TerraSAR-X intensity and interferometric coherence," *J. Photogramm. Remote Sens.*, vol. 152, pp. 178–191, Jun. 2019.
[13] T. G. J. Rudner *et al.*, "Multi3Net: Segmenting flooded buildings via fusion of multiresolution, multisensor, and multitemporal satellite imagery," in *Proc. Conf. Artif. Intell. (AAAI)*, vol. 33, no. 1, Jul. 2019, pp. 702–709.
[14] D. Xiang, T. Tang, Y. Ban, Y. Su, and G. Kuang, "Unsupervised polarimetric SAR urban area classification based on model-based decomposition with cross scattering," *J. Photogramm. Remote Sens.*, vol. 116, pp. 86–100, Jun. 2016.
[15] Y. Yamaguchi, A. Sato, W.-M. Boerner, R. Sato, and H. Yamada, "Four-component scattering power decomposition with rotation of coherency matrix," *IEEE Trans. Geosci. Remote Sens.*, vol. 49, no. 6, pp. 2251–2258, Jun. 2011.
[16] M. Chini, R. Pelich, R. Hostache, P. Matgen, and C. Lopez-Martinez, "Towards a 20 m global building map from Sentinel-1 SAR data," *Remote Sens.*, vol. 10, p. 1833, Nov. 2018.
[17] M. Chini, R. Hostache, L. Giustarini, and P. Matgen, "A hierarchical split-based approach for parametric thresholding of SAR images: Flood inundation as a test case," *IEEE Trans. Geosci. Remote Sens.*, vol. 55, no. 12, pp. 6975–6988, Dec. 2017.